Available online at www.sciencedirect.com
ScienceDirect
Journal of Power Sources 160 (2006) 258–267
JOURNAL OF POWER SOURCES
www.elsevier.com/locate/jpowsour

Development of a control-oriented model for the solid oxide fuel cell

Xiongwen Zhang, Jun Li, Guojun Li *, Zhenping Feng

School of Energy and Power Engineering, Xi'an Jiaotong University, Shaanxi, China

Received 9 November 2005; received in revised form 25 December 2005; accepted 5 January 2006
Available online 20 February 2006

Abstract

A lumped, non-linear control-oriented dynamic model for the solid oxide fuel cell has been developed. The exponential decay function and the exponential associate function are introduced to fit the distribution characteristics of fuel cell state variables in the flow direction of the gases in order to account for the effect of spatial variation of fuel cell parameters in the dynamic model. It is integrated into the dynamic model by three characteristic parameters of the fitting function, which are determined via numerical simulations. A planar solid oxide fuel cell with co-flow has been used to evaluate the accuracy and applicability of the current dynamic model. The dynamic model is programmed and implemented using the SIMULINK software. The simulation results indicate the model has good service quality to predict the state variables and the performance of the solid oxide fuel cell.

Keywords: Solid oxide fuel cell; Control-oriented dynamic model; Fitting functions

1. Introduction

The solid oxide fuel cell (SOFC) is a promising energy conversion device because of its high efficiency, environmental compatibility and modularity. SOFCs will play a significant role in the power generation market in the future. The control technology is critical in its development and is an important factor for commercializing the SOFC. A reliable and accurate control-oriented model is of great importance to understand the dynamic characteristics of the SOFC.

Control techniques based on process models require simple and accurate differential and algebraic equations to represent the device dynamic response characteristics. Up to now, there have been many publications [1–5] on the dynamic models of the SOFC. The characteristics of the fuel cell have been simulated by the dynamic models [1,2] at the cell level according to spatial variations. Discretization of the computational slice element along the streamwise direction was used to formulate each balance of material and energy. It is very difficult to apply these dynamic models to a controlling study of the fuel cell because the spatial variations of fuel cell parameters are included in these dynamic models. Lukas et al. [3,4] and Padulles et al. [5] introduced non-linear zero-dimensional, single node lumped dynamic models which are suitable for fuel cell control systems. However the spatial effect on the fuel cell performance was not taken into account in their models. The distributions of the gaseous molar fractions and temperature were assumed to be uniform within the whole stack in the zero-dimensional dynamic model. In fact, the distribution of these variables is non-uniform for most SOFC configurations. For example, the H_2 molar fraction increases firstly and then decreases along the fuel flow direction in the internal reforming SOFC. The performance of the SOFC depends strongly on the distributions of the gaseous molar fractions and the temperature. Thus, the accuracy of the zero-dimensional dynamic model reported in the literature [3–5] is not high for predicting the fuel cell performances. Comte et al. [6] claimed that the zero-dimensional dynamic model could lead to as high as a 20% error compared with the more complex model in predicting the thermal and power outputs for the planar SOFC with cross-flow. Thus the spatial effect on the fuel cell performance should be taken in account to improve the accuracy of the dynamic model.

* Corresponding author. Tel.: +86 29 82668728; fax: +86 29 82665062.
E-mail address: liguojun@mail.xjtu.edu.cn (G. Li).

0378-7753/$ – see front matter © 2006 Elsevier B.V. All rights reserved.
doi:10.1016/j.jpowsour.2006.01.024

Nomenclature

A_1, A_2	the parameter of exponential fitting function
A_e	fuel cell active area (m^2)
A_r	reforming reaction surface area (m^2)
A_s	anode section area (m^2) (upright with the gas flow direction)
A_v	volume section area (m^2) (upright with the gas flow direction)
c_p	specific heat capacity ($J\,mol^{-1}\,K$)
E	theoretical Nernst potential (V)
E_A	activation energy ($J\,mol^{-1}$)
f_r	the reforming reaction balance constant
F	Faraday constant (=96485 $C\,mol^{-1}$)
h	molar enthalpy ($J\,mol^{-1}$)
ΔH_1	total change of enthalpy for the electrochemical reaction
ΔH_2	total change of enthalpy for the fuel reforming reaction
ΔH_3	total change of enthalpy for the gas–water shift reaction
i	current density ($A\,m^{-2}$)
i_0	exchange current density ($A\,m^{-2}$)
i_L	diffusion limiting current density ($A\,m^{-2}$)
k	derivative of fitting function at the point (0, $y(0)$)
k_r, k_s	reforming chemical reaction constant (=4274 $mol\,s^{-1}\,m^2$ bar), shift gas–water chemical reaction constant (=1.2×10^4 $mol\,m^3\,s^{-1}$)
K	equilibrium constant
L	fuel cell length (m)
M	molecular mass
$\dot{n}$	molar flux ($mol\,s^{-1}$)
n_e	electrons transferred per reaction
P	operating pressure (Pa)
P_0	standard pressure (Pa)
Q	molar chemical reaction heat ($J\,mol^{-1}$)
Q_{chem}	volumetric chemical reaction produced heat ($J\,s^{-1}\,m^{-3}$)
Q_{gen}	generated heat ($J\,s^{-1}$)
$\dot{r}$	volumetric reaction rate ($mol\,s^{-1}\,m^{-3}$)
R	universal gas constant (=8.314 $J\,mol^{-1}\,K^{-1}$)
R_e	electrolyte ohmic resistance (Ω)
S	source component
T	temperature (K)
t	time (s)
t_1, t_2	fitting function exponential parameter
U	voltage (V)
V	velocity ($m\,s^{-1}$)
x	gaseous molar fraction
y	fitting function
z	dimensionless spatial coordinate of gas flow direction ($z = (z^*/L) \in [0, 1]$)
z^*	spatial coordinate of gas flow direction

Greek letters

η	number of gas
λ	heat conductivity ($W\,m^{-1}\,K^{-1}$)
μ	fluid viscosity ($kg\,m\,s^{-1}$)
Φ	electric potential (V)
ρ	density ($kg\,m^{-3}$)
σ	conductivity ($S\,m^{-1}$)
ξ	number of chemical reaction
ζ	correction coefficient for gas-water shift reaction rate (=1.25)

Subscripts

a	anode
c	cathode
CH_4	methane
CO	carbon monoxide
CO_2	carbon dioxide
e	electrochemical reaction
H_2	hydrogen
H_2O	water (gas)
i	chemical
j	the jth chemical reaction
N_2	nitrogen
O_2	oxygen
ohm	ohmic
r	reforming chemical reaction
rad	radiant
s	gas–water shift chemical reaction

Superscripts

−	mean value
in	fuel cell inlet
out	fuel cell outlet
s	solid

Based on the single node, a control-oriented dynamic model of SOFC stack is developed in this study. The distribution characteristics of gaseous molar fractions and temperature are determined using numerical simulation in order to lump the spatial effect into the model. The exponential decay function and the exponential association function are used to fit the numerical simulation data for these variables in the flow direction of the gases. A dynamic model with parameters for the fitting function determined from numerical data is developed in current study. The spatial effect on the SOFC performance is considered in the present model via the parameters in the fitting functions. The present dynamic model has been programmed in MATLAB/SIMULINK. The reliability and accuracy of the current dynamic model is demonstrated through a planar SOFC dynamic simulation.

2. Dynamic model development

2.1. Chemical processes

The electrochemical process in a SOFC is illustrated in Fig. 1. Fuel and air flow into the cell separately. They diffuse through

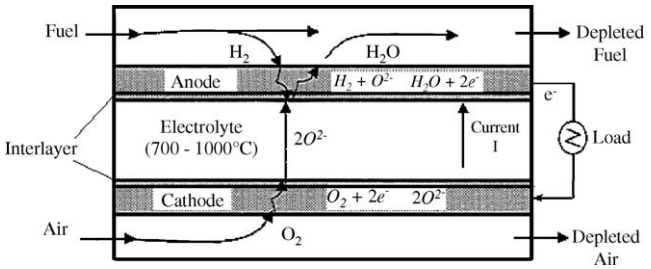

Fig. 1. Electrochemical processes within SOFC.

the porous electrode structure to the interlayer and are then adsorbed. At the cathode interlayer, oxygen is reduced by incoming electrons to produce oxygen anions. The oxygen anions are conducted through the electrolyte to the anode interlayer where they electrochemically combine with the adsorbed hydrogen to form water and release electrons to the external circuit. The electrochemical reactions for the anode and cathode are described as

anode side : $H_2 + O^{2-} \rightarrow H_2O + 2e^-$

cathode side : $1/2O_2 + 2e \rightarrow O^2$

overall reaction : $1/2O_2 + H_2 \rightarrow H_2O$.

For the internal reforming of SOFC, the reforming reaction and gas-shift reaction are included in the model:

steam-reforming : $CH_4 + H_2O \rightarrow CO + 3H_2$

shifting : $CO + H_2O = CO_2 + H_2$

Also, the electrochemical oxidation of carbon monoxide at the anode is formulated as

$CO + O^{2-} \rightarrow CO_2 + 2e^-$.

This reaction speed is 2–5 times slower than that of hydrogen. The rapid gas-shift reaction becomes the dominant reaction [7,8]. Thus, the oxidation of carbon monoxide is neglected in the present model.

2.2. Model development

The gaseous molar fractions and the temperature at the outlet position of gas channels are chosen as state variables in the present study. The steam reforming reaction is very fast at a short distance from the fuel inlet in the internal reforming design SOFC. Consequently, the reactants of the reforming reaction CH_4 and H_2O concentrations rapidly decrease and the product H_2 and CO concentrations increase within this area. Then H_2 decreases gradually as a result of consumption by the electrochemical oxidation while flowing towards the channel outlet. The exponential decay function and the exponential associate function are applied to describe the above characteristics in this work. The curves of the functions are plotted in Fig. 2. The exponential decay function and exponential associate function are formulated by function (1) and (2), respectively. The distribution of the gaseous molar fractions and temperature can be fitted through adjusting the parameters of the formulation (1) and (2).

$$y = y_0 + (A_1 e^{-z/t_1} + A_2 e^{-z/t_2}) \quad (1)$$

$$y = y_0 + [A_1(1 - e^{-z/t_1}) + A_2(1 - e^{-z/t_2})] \quad (2)$$

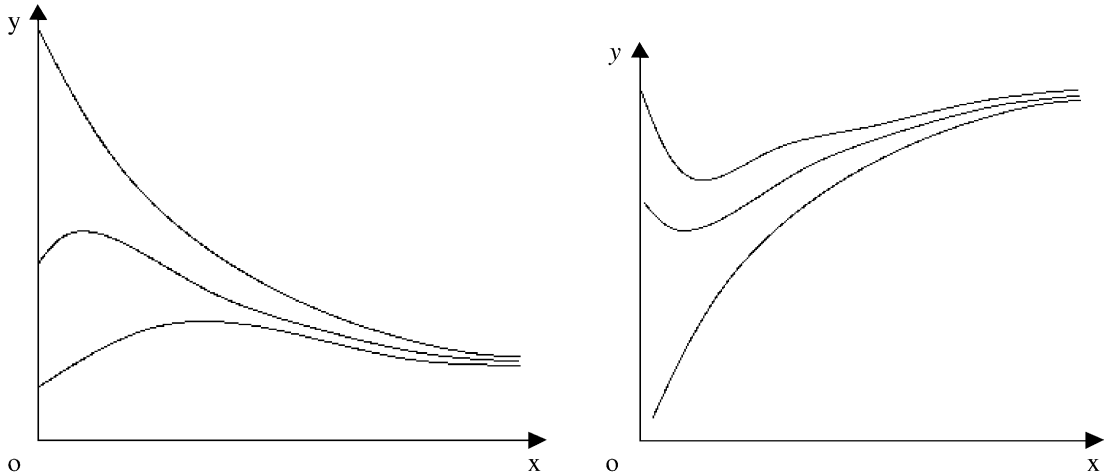

Fig. 2. The fitting functions curve character. (a) Exponential decay function: $y = y_0 + A_1 e^{-x/t_1} + A_2 e^{-x/t_2}$. (b) Exponential associate function $y = y_0 + A_1(1 - e^{-x/t_1}) + A_2(1 - e^{-x/t_2})$.

For the exponential decay function, there exists the following condition at the SOFC gases inlet:

$$y(0) = y_0 + A_1 + A_2 \tag{3}$$

Similarly, at the outlet:

$$y(1) = y_0 + A_1\,\mathrm{e}^{-1/t_1} + A_2\,\mathrm{e}^{-1/t_2} \tag{4}$$

At the point (0, $y(0)$), the derivative is defined as k and is given by

$$k = -\frac{A_1}{t_1} - \frac{A_2}{t_2} \tag{5}$$

Combine the Eqs. (3)–(5); the parameters y_0, A_1, A_2 can be expressed as follows:

$$y_0 = y(0) + kt_1 + \frac{kt_1(t_1 - t_2)(1 - \mathrm{e}^{-1/t_1})}{\Delta} + \frac{t_1 - t_2}{\Delta}(y(0) - y(1)) \tag{6}$$

$$A_1 = -kt_1 - \frac{t_1}{\Delta}(y(0) - y(1)) - \frac{kt_1^2(1 - \mathrm{e}^{-1/t_1})}{\Delta} \tag{7}$$

$$A_2 = \frac{t_2}{\Delta}(y(0) - y(1)) + \frac{kt_1t_2(1 - \mathrm{e}^{-1/t_1})}{\Delta} \tag{8}$$

where

$$\Delta = t_2(1 - \mathrm{e}^{-1/t_2}) - t_1(1 - \mathrm{e}^{-1/t_1}).$$

Similarly, for the exponential associate function, the parameters y_0, A_1, A_2 are given as

$$y_0 = y(0) \tag{9}$$

$$A_1 = kt_1 + \frac{t_1}{\Delta}(y(0) - y(1)) + \frac{kt_1^2(1 - \mathrm{e}^{-1/t_1})}{\Delta} \tag{10}$$

$$A_2 = -\frac{t_2}{\Delta}(y(0) - y(1)) - \frac{kt_1t_2(1 - \mathrm{e}^{-1/t_1})}{\Delta} \tag{11}$$

where

$$k = \frac{A_1}{t_1} + \frac{A_2}{t_2} \tag{12}$$

The averaged value of y is calculated by

$$\bar{y} = \int_0^1 y(z)\,\mathrm{d}z = y_0 - A_1t_1(\mathrm{e}^{-1/t_1} - 1) - A_2t_2(\mathrm{e}^{-1/t_2} - 1)$$

for the exponential decay function, (13)

$$\bar{y} = \int_0^1 y(z)\,\mathrm{d}z = y_0 - A_1(1 + t_1\,\mathrm{e}^{-1/t_1} - t_1) - A_2(1 + t_2\,\mathrm{e}^{-1/t_2} - t_2)$$

for the exponential associate function. (14)

Substituting Eqs. (6)–(8) and Eqs. (9)–(11) into Eqs. (13) and (14), respectively. The variable $\bar{y}$ for both cases has the same form as

$$\bar{y} = \varphi_1 y(0) + \varphi_2 y(1) + \varphi_3 \tag{15}$$

where

$$\varphi_1 = 1 + \frac{t_1(1 + t_1\,\mathrm{e}^{-1/t_1} - t_1) - t_2(1 + t_2\,\mathrm{e}^{-1/t_2} - t_2)}{\Delta},$$

$$\varphi_2 = \frac{t_2(1 + t_2\,\mathrm{e}^{-1/t_2} - t_2) - t_1(1 + t_1\,\mathrm{e}^{-1/t_1} - t_1)}{\Delta},$$

$$\varphi_3 = kt_1(1 + t_1\,\mathrm{e}^{-1/t_1} - t_1) + \frac{kt_1^2(1-\mathrm{e}^{-1/t_1})(1+t_1\,\mathrm{e}^{-1/t_1}-t_1)}{\Delta} - \frac{kt_1t_2(1 - \mathrm{e}^{-1/t_1})(1 + t_2\,\mathrm{e}^{-1/t_2} - t_2)}{\Delta}.$$

2.2.1. Mass balance equations

Each gas material balance equation is written as

$$\frac{PV}{RT}\frac{\mathrm{d}\bar{x}_i}{\mathrm{d}t} = \dot{n}^{\mathrm{in}}x_i(0) - \dot{n}^{\mathrm{out}}x_i(1) + \sum_{j=1}^{\xi}\gamma_{i,j}\bar{R}_j \tag{16}$$

where i and j denote the ith gas and the jth independent reactions. Changing y into x_i for Eq. (15) and substituting it into Eq. (16), then

$$\frac{\varphi_{2,i}PV}{R\bar{T}}\frac{\mathrm{d}x_i(1)}{\mathrm{d}t} = \dot{n}^{\mathrm{in}}x_i(0) - \dot{n}^{\mathrm{out}}x_i(1) + \sum_{j=1}^{\xi}\gamma_{i,j}\bar{R}_j. \tag{17}$$

Three chemical reactions are included in the presented model. The calculation of the reactive rate is given as follows:

$$\bar{R}_1 = A_{\mathrm{e}}\frac{\bar{i}}{n_{\mathrm{e}}F} \tag{18}$$

$$\bar{R}_2 = A_{\mathrm{r}}k_{\mathrm{r}}f_{\mathrm{r}}P\int_0^1 x_{\mathrm{CH_4}}\exp\left(-\frac{E_{\mathrm{A}}}{RT}\right)\mathrm{d}z \tag{19}$$

$$\bar{R}_3 = \zeta A_{\mathrm{s}}k_{\mathrm{s}}P\int_0^1 (x_{\mathrm{CO}}x_{\mathrm{H_2O}} - K_{\mathrm{shift}}x_{\mathrm{CO_2}}x_{\mathrm{H_2}})\,\mathrm{d}z \tag{20}$$

K_{shift} is obtained using the method of Ref. [9]. The outlet of total molar number is calculated by the continuity equations as described in the following forms:

$\dot{n}^{\mathrm{out}} = \dot{n}^{\mathrm{in}} + 2\bar{R}_2$ for the anode side,

$\dot{n}^{\mathrm{out}} = \dot{n}^{\mathrm{in}} - \frac{1}{2}\bar{R}_1$ for the cathode side.

The matrix form for the mass balance equations is written as follows:

$$C\dot{x} = Ax + B \tag{21}$$

where

$$x = [x_1(1)x_2(1)\dots x_\eta(1)]^T,$$

$$C = \frac{PV}{R\bar{T}}\begin{bmatrix} \varphi_{2,1} & 0 & 0 & \dots & 0 \\ 0 & \varphi_{2,2} & 0 & \dots & 0 \\ 0 & 0 & \varphi_{2,3} & \dots & 0 \\ 0 & 0 & 0 & \ddots & 0 \\ 0 & 0 & 0 & \dots & \varphi_{2,\eta} \end{bmatrix},$$

$$A = -n^{\text{out}}\begin{bmatrix} 1 & 0 & 0 & \dots & 0 \\ 0 & 1 & 0 & \dots & 0 \\ 0 & 0 & 1 & \dots & 0 \\ 0 & 0 & 0 & \ddots & 0 \\ 0 & 0 & 0 & \dots & 1 \end{bmatrix},$$

$$B = -n^{\text{in}}\begin{bmatrix} x_1(0) + \sum_{j=1}^{\xi}\gamma_{1,j}\bar{R}_j \\ x_2(0) + \sum_{j=1}^{\xi}\gamma_{2,j}\bar{R}_j \\ \vdots \\ x_\eta(0) + \sum_{j=1}^{\xi}\gamma_{\eta,j}\bar{R}_j \end{bmatrix}$$

$$\bar{T} = \varphi_{1,T}T(0) + \varphi_{2,T}T(1) + \varphi_{3,T} \tag{22}$$

where

$$\sum_{i=1}^{\eta} x_i(1) = 1$$

2.2.2. Energy balance equation

The temperature dynamic model is acquired from the energy conservation equation. The assumption that the temperature distribution meets the one-dimensional distribution along the flow direction is similar to the molar fractions assumption. The gases thermal capacity is calculated separately for the fuel and the air. The energy conservation equation is given as

$$M^{\text{s}}c_p^{\text{s}}\frac{\mathrm{d}\bar{T}}{\mathrm{d}t} + \sum_{k=1}^{2}\sum_{i=1}^{\eta_k}\frac{\mathrm{d}\bar{h}_i\bar{n}_i}{\mathrm{d}t} = \sum_{k=1}^{2}\sum_{i=1}^{\eta_k}[\dot{n}_i(0)h_i(0) - \dot{n}_i(1)h_i(1)] + Q_{\text{gen}} \tag{23}$$

where

$\eta_1 = 5$ for H_2, H_2O, CO, CO_2, CH_4 while $k = 1$, $\eta_2 = 2$ for O_2, N_2 while $k = 2$.

Assuming the gas specific heat is a function of the average temperature $\bar{T}$ and the thermodynamic properties of the mixture gases satisfy the ideal gas mixture law. Then

$$\left[M^{\text{s}}c_p^{\text{s}} + \frac{P}{R\bar{T}}\sum_{k=1}^{2}\left(A_{\text{v},k}\sum_{i=1}^{\eta_k}c_{pi}\bar{x}_i\right)\right]\frac{\mathrm{d}\bar{T}}{\mathrm{d}t} = \sum_{k=1}^{2}\sum_{i=1}^{\eta_k}c_{pi}[\dot{n}_k^{\text{in}}x_i(0)T(0) - \dot{n}^{\text{out}}x_i(1)T(1)] - \sum_{k=1}^{2}\sum_{i=1}^{\eta_k}\bar{h}_i\frac{\mathrm{d}\bar{n}_i}{\mathrm{d}t} + Q_{\text{gen}}. \tag{24}$$

The response time of gas molar fraction is much faster than that of temperature. Therefore, the second term on the right-hand side of Eq. (24) can be neglected. Expanding the left terms and the Eq. (24) becomes

$$\varphi_{2,T}\left[M^{\text{s}}c_p^{\text{s}} + \frac{P}{R\bar{T}}\sum_{k=1}^{2}\left(A_{\text{v},k}\sum_{i=1}^{\eta_k}c_{pi}\bar{x}_i\right)\right]\frac{\mathrm{d}T(1)}{\mathrm{d}t} = \sum_{k=1}^{2}\sum_{i=1}^{\eta_k}c_{pi}\left[\dot{n}_k^{\text{in}}x_i(0)T(0) - \dot{n}_k^{\text{out}}x_i(1)T(1)\right] + Q_{\text{gen}} \tag{25}$$

where

$$Q_{\text{gen}} = \Delta H_1\bar{R}_1 + \Delta H_2\bar{R}_2 + \Delta H_3\bar{R}_3 - \bar{P}_{\text{dc}}.$$

2.2.3. Voltage model

The Nernst potential is calculated as a function of current density, operating pressure, temperature and the gases molar fraction. The irreversibility in the voltage drop is contributed by

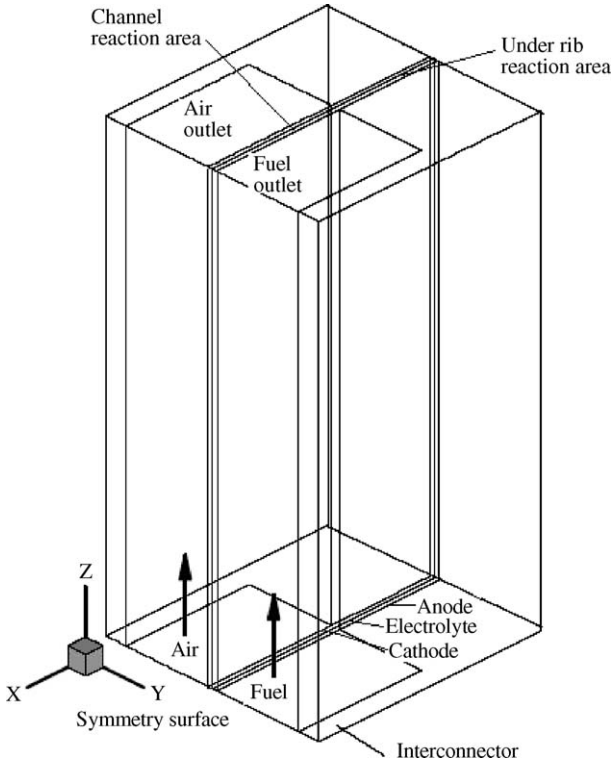

Fig. 3. The geometry of the half single-unit cell for the co-flow planar SOFC.

Table 1
The diffuse coefficient and source terms for the governing equations

	Diffuse coefficient (Γ_ϕ)	Source terms (S_a)	
		Electrode	Interlayer
Mass	0		anode side : $M_{H_2O}\gamma_{H_2O,1}R_1 + M_{H_2}\gamma_{H_2,1}R_1$, cathode side : $M_{O_2}\gamma_{O_2,1}R_1$
N–S	μ	$-(\mu/\alpha)\vec{V}$	$-(\mu/\alpha)\vec{V}$
	$\rho D_{i,m}$	$M_i(\gamma_{i,2}R_2 + \gamma_{i,2}R_3)$	$M_i(\gamma_{i,1}R_1 + \gamma_{i,2}R_2 + \gamma_{i,3}R_3)$
Electric potential	σ		anode side: $-i$, cathode side: i
Energy	μ/P_r	$Q_{ohm} + Q_{rad}$	$Q_{ohm} + Q_{chem} + Q_{rad}$

Table 2
Material properties and operating conditions [11,12]

	Cathode	Electrolyte	Anode	Interconnect
σ	$\frac{4.2\times10^7}{T}\exp\left(-\frac{1200}{T}\right)$	$3.34\times10^4\exp\left(-\frac{10300}{T}\right)$	$\frac{9.5\times10^7}{T}\exp\left(-\frac{1150}{T}\right)$	$\frac{9.3\times10^6}{T}\exp\left(-\frac{1100}{T}\right)$
λ	3	2	3	3.5
ρ		6600		
c_p		400		
Operating conditions				
Operating voltage (V)			0.65	
Operating pressure (bar)			1	
Inlet gas temperature (K)			1173	
Inlet gas composition	Air: O_2 21%, N_2 79%; fuel: H_2 26.26%, H_2O 49.34%, CO 2.94%, CO_2 4.36%, CH_4 17.10%			

Table 3
comparisons of the numerical simulation results with IEA benchmark

	Voltage	Average current density	Maximum temperature	Minimum temperature	Fuel utilization
Benchmark	0.633–0.649	3000	1294–1307	1120–1135	85%
Simulation	0.65	2959	1301	1139	83%

Table 4
The fitting function parameters for each of state variables

	x_{H_2}	x_{O_2}	x_{H_2O}	x_{CO}	x_{CO_2}	x_{CH_4}	x_{N_2}	T
t_1	0.12012	0.98607	0.10457	0.08696	23.20000	0.10269	9.60000	0.08372
t_2	0.80000	0.29651	1.82261	1.65348	17.90000	0.03254	9.50000	0.92091
k	2.90000	−0.01510	−2.30000	1.22000	0.11564	−2.50000	0.02682	−815.00000

three kinds of polarization losses named the activation, concentration and ohmic overpotentials. The Nernst equation for the SOFC is:

$$E = \frac{R\bar{T}}{n_e F}\ln K(\bar{T}) - \frac{R\bar{T}}{2n_e F}\ln\left[\frac{\bar{x}_{H_2O}^2 P_0}{\bar{x}_{H_2}^2 \bar{x}_{O_2}}\right] \quad (26)$$

where $P_a = P_c = P$ is assumed. Subtracting the electrochemical losses and the output voltage is given by

$$U = E - \bar{i}R_e(\bar{T}) - \frac{2R\bar{T}}{n_e F}\sinh^{-1}\left(\frac{\bar{i}}{2i_{0a}}\right) - \frac{2R\bar{T}}{n_e F}\sinh^{-1}\left(\frac{\bar{i}}{2i_{0c}}\right) + \frac{R\bar{T}}{n_e F}\ln\left(1-\frac{\bar{i}}{i_L}\right) \quad (27)$$

Table 5
Comparison of the value of dynamic model prediction with numerical simulation for the variables

	x_{H_2}	x_{O_2}	x_{H_2O}	x_{CO}	x_{CO_2}	x_{CH_4}	x_{N_2}	T	U
Dynamic model prediction	0.08384	0.1854	0.7343	0.0563	0.1255	6.0e−5	0.8146	1304	0.655
Numerical simulation (average values)	0.1124	0.183	0.7055	0.027	0.1549	2.0e−4	0.817	1301	0.65

where the second term on the right-hand side of the above equation is ohmic loss, the third term is activation loss at the anode side, the fourth term is activation loss at the cathode side, and the last term is concentration loss.

3. Model evaluation

The dynamic response performance of a planar SOFC with co-flow designed with the direct internal reforming method is

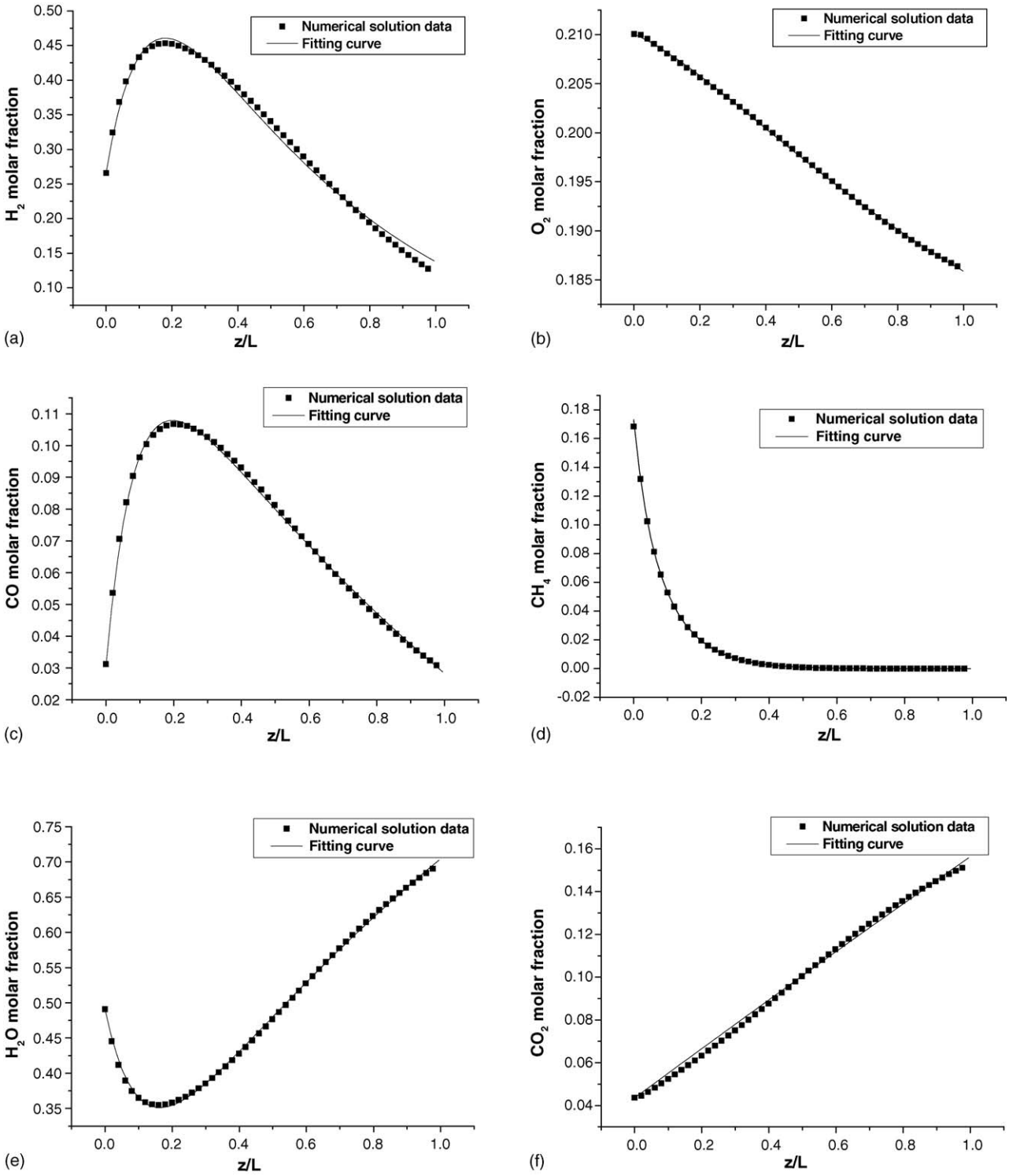

Fig. 4. Non-linear curve fitting using the exponential decay function and exponential association function for the gas molar fraction and the temperature along the gases flow direction in the gas channel: (a) H_2; (b) O_2; (c) CO; (d) CH_4; (e) H_2O; (f) CO_2; (g) N_2; (h) temperature.

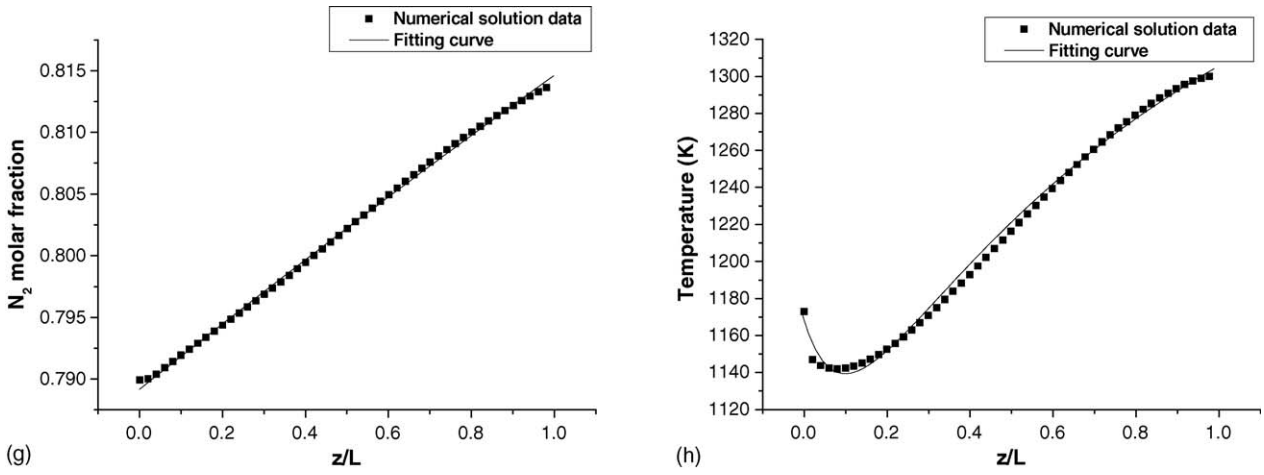

Fig. 4. (*Continued*).

simulated to demonstrate the reliability and accuracy of the present dynamic model. This fuel cell stack was designed as a modeling excise, which was launched by the International Energy Agency (IEA) involving seven Europeans countries and Japan in 1995 [12].

The spatial distributions of state variables in the SOFC are calculated by solving the three-dimensional Navier–Stokes equations combined with gases transport equations. The numerical results are used to find the parameters t_1, t_2, and k of the fitting function in the present dynamic model. Different values of t_1, t_2, and k are obtained for each gas species and temperature spatial distribution in this case. The numerical method for solving three-dimensional Navier–Stokes equations and gases transport equations is briefly described in later section.

3.1. Numerical simulations

The governing equation for the steady operation can be written as follows:

$$\mathrm{div}(\rho\vec{V}\phi) = \mathrm{div}(\Gamma_\phi \,\mathrm{grad}\,\phi) + S_\phi + S_\mathrm{a} \tag{28}$$

where ϕ is a generic variable.

The diffusion coefficient and source terms S_a are summarized in Table 1. The source term S_a for energy equation is the sum of the ohmic heat, the chemical reaction heat and the radiant heat exchange. The discrete ordinate radiation model is applied to calculate the radiant heat exchange [10] in present numerical simulation. The ohmic heat is calculated by the following formulae:

$$Q_\mathrm{ohm} = \sigma \,\mathrm{grad}\,\Phi \,\mathrm{grad}\,\Phi \tag{29}$$

At the interlayer, the chemical reaction heat is calculated by

$$Q_\mathrm{chem} = \dot{r}_\mathrm{e} Q_\mathrm{e} + \dot{r}_\mathrm{r} Q_\mathrm{r} + \dot{r}_\mathrm{s} Q_\mathrm{s} \tag{30}$$

The electrochemical thermodynamic models are shown in Eqs. (26) and (27).

The given parameters in present numerical simulation are specified in Table 2. The flow is assumed to be laminar because the Reynolds number is very low ($Re < 100$) in this case. The governing equations including continuity, momentum conservation, transport, energy conservation, and electric potential are solved using the computational fluid dynamics software Fluent 6.1. Thermodynamic equations for the electrochemical reactions are incorporated and solved by user-defined functions (UDFs), which are provided by Fluent 6.1. The governing equations are discretized with second order upwind format using control volume method. Half of the single-unit is simulated because of symmetry.

Half of the single-unit cell planar SOFC is illustrated in Fig. 3. The geometrical parameters of the single-unit cell planar SOFC are given in [11] and are summarized as follows: active area: 5.42×100 mm, anode thickness: 50 μm, cathode thickness: 50 μm, electrolyte thickness: 150 μm, channel height: 1 mm, rib width: 2.42 mm, and bipolar plate thickness: 2.5 mm. The permeability of porous for electrode is 1.0×10^{-8} m^{-2}. And its porosity is 0.2.

Table 3 gives the comparison of current numerical simulation results with the data given by the IEA. As shown in Table 3, the numerical simulation results agree with the IEA benchmark values. This indicates that the accuracy of the results obtained by numerical simulation with current model is reliable.

3.2. Dynamic simulation

The parameters of fitting functions t_1, t_2, and k must be determined before the present dynamic model can be implemented. The kind of functions used in the curve fitting is decided according to the distribution characteristics of each state variable. In this paper, only the state variable distribution characteristics within the channel area are fitted by the introduced fitting functions. The exponential decay function is employed for the molar fraction of H_2, O_2, CO, CH_4. The exponential association function is employed for the molar fractions of H_2O, CO_2, N_2 and the temperature.

Fig. 4(a)–(d) shows the fitting curves of molar fraction of H_2, O_2, CO, CH_4 using the exponential decay function. Fig. 4(e)–(h) shows the fitting curves of the molar fractions of H_2O, CO_2, N_2

and the temperature using the exponential association function. The solid lines in Fig. 4 are the fitted functions using the numerical simulation results. As shown in Fig. 4, the fitting curves well represent the numerical results with the solid curves very close to the numerical data at all points, which represent the distribution characteristics of state variables along the gases streamwise. The fitting functions parameters A_1, A_2, t_1, and t_2 for each of state variables are then determined. The parameter k is calculated by Eq. (5) for molar fraction of H_2, O_2, CO, CH_4 and by Eq. (12) for the molar fractions of H_2O, CO_2, N_2 and the temperature,

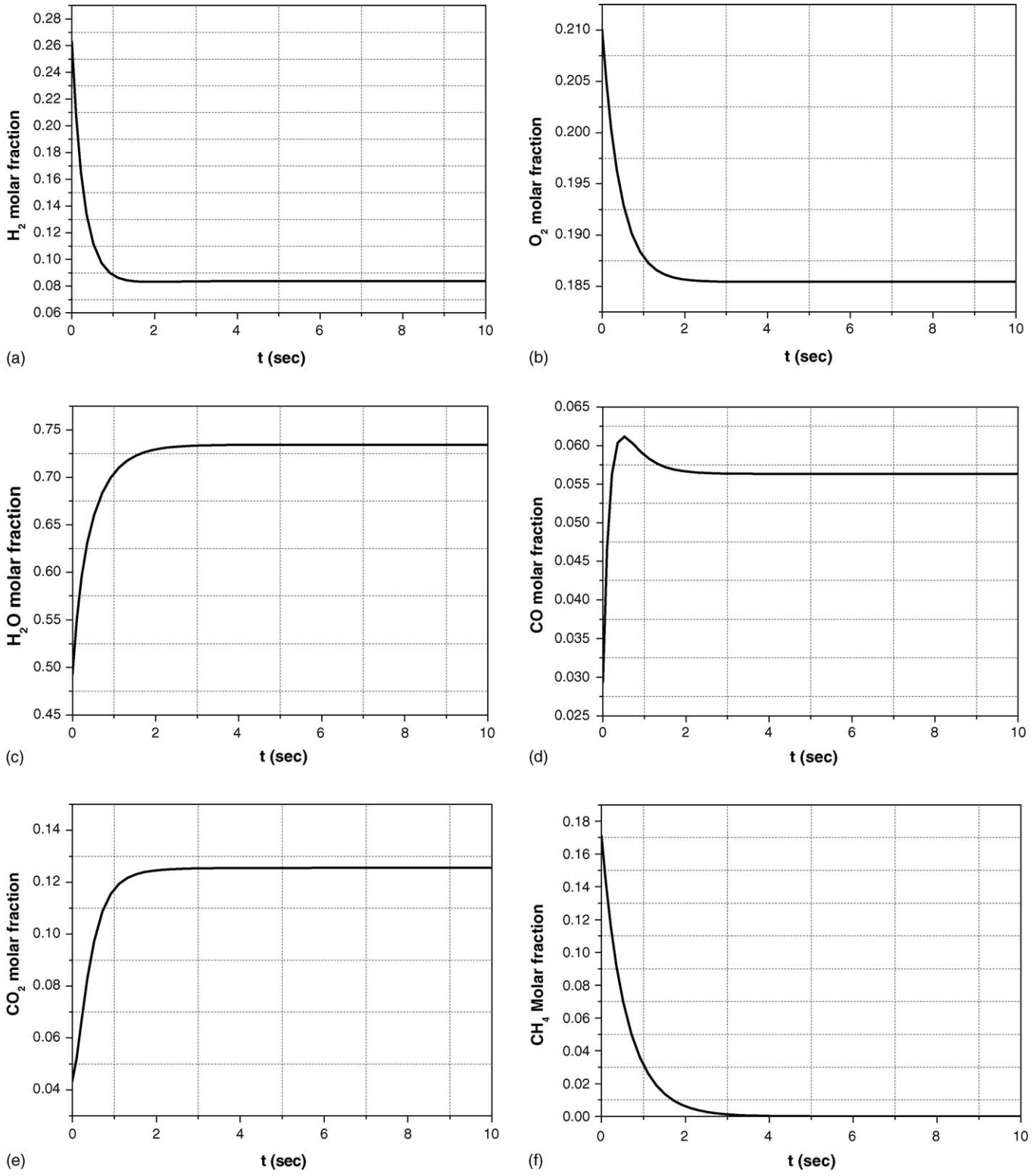

Fig. 5. The response of state variables and the performance for the planar co-flow SOFC: (a) H_2; (b) O_2; (c) H_2O; (d) CO; (e) CO_2; (f) CH_4; (g) temperature; (h) voltage.

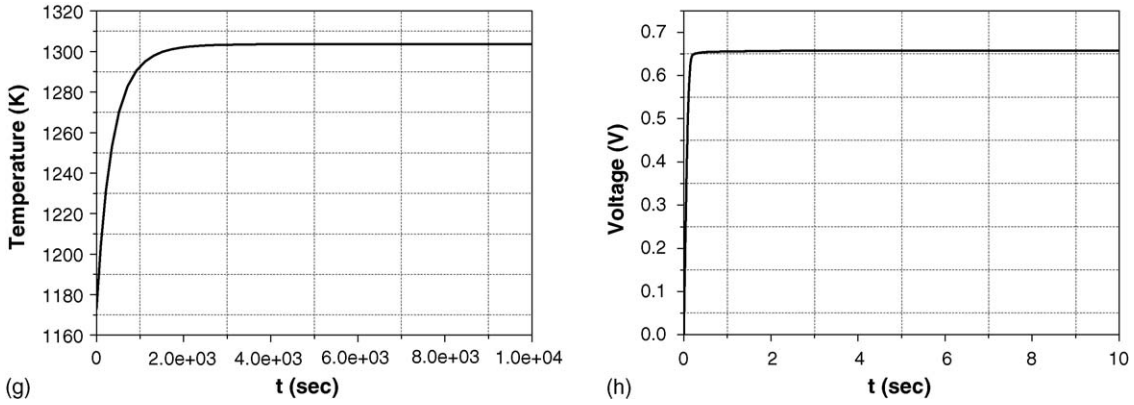

Fig. 5. (*Continued*).

respectively. The values of t_1, t_2 and k for each of state variable are presented in Table 4.

The dynamic simulation is implemented using SIMULINK. The inlet gaseous molar fractions, the inlet temperature, the averaged current density, and the fuel utilization are specified as input parameters. The material properties are identical to the numerical simulation used. Table 5 shows the comparison of steady value of present dynamic simulation with the data obtained by numerical simulation. In Table 5, the numerical data are the outlet average values of each state variable. The voltage is the fuel cell output voltage. It can be seen from Table 5 that the value of dynamic model prediction for x_{O_2}, x_{N_2}, x_{CH_4}, T and U is consistent with that of numerical solution. The differences between the value of dynamic model prediction and the numerical simulation results for x_{H_2}, x_{H_2O}, x_{CO} and x_{CO_2} are less than 0.03 comparing the numerical simulation results. This difference is caused by the interconnector rib effect. As shown in Fig. 3, for the underneath interconnector rib reaction area, the gaseous species are transported only by diffusion in the porous electrodes. This leads to a big difference of gaseous molar fractions between the underneath interconnector rib reaction area and the channel reaction area. In the dynamic model, the parameters of fitting functions only reflect the distribution of gaseous molar fractions in the channel reaction area. This causes errors in the prediction of gas-shift reaction rate. Present dynamic model only uses a correction coefficient ζ in Eq. (20) to correct the gas-shift reaction rate. This cannot completely reflect the difference of gaseous molar fractions between the channel reaction area and the underneath interconnector reaction area.

Fig. 5 shows the transient response of state variables for the steady-state operation. Most of the state variables are first order response except the CO molar fraction which is a second order term. The time constant of thermal response is much larger than that of gaseous molar fractions. And the output voltage has the minimum time constant.

4. Conclusion

A non-linear control-oriented dynamic model has been developed based on the assumption that the variables follow a one-dimensional distribution. Two kinds of fitting function, namely the exponent decay function and the exponent associate function were introduced to fit the distribution characteristics of the gaseous molar fractions and temperature along the streamwise direction. The spatial effect has been lumped into the dynamic model by fitting the three parameters t_1, t_2, and k of the used function. These parameters are determined through numerical simulations.

A co-flow configuration planar SOFC has been introduced to evaluate the developed model. The dynamic model has been implemented on this planar SOFC using SIMULINK software. The simulation results show that the present dynamic model has a good predictive quality for the state variable responses and fuel cell performance.

Acknowledgments

The research work was sponsored by the Doctor Foundation of Xi'an Jiaotong University (No. DFXJTU2005-01) and the National High Technology Research and Development Program of China (No. 2002AA503020).

References

[1] R.S. Gemmen, E. Liese, J.G. Rivera, F. Jabbari, J. Brouwer, Proceedings of the ASME Turbo Expo, Munich, Germany, 2000 (GT0-554).
[2] R.A. Roberts, F. Jabbari, J. Brouwer, R.S. Gemmen, E.A. Liese, Proceedings of the ASME Turbo Expo, Georgia, USA, 2003 (GT-38774).
[3] M.D. Lukas, K.Y. Lee, H. Ghezel-Ayagh, IEEE Trans. Energy Convers. 14 (1999) 1651.
[4] M.D. Lukas, K.Y. Lee, H. Ghezel-Ayagh, IEEE Trans. Energy Convers. 16 (2001) 289.
[5] J. Padulles, G.W. Ault, J.R. McDonald, J. Power Sources 86 (2000) 495.
[6] A. Comte, Ph. Matheron, Ph. Stevens, Proceedings of the Third European SOFC Form, Nantes, France, 1998.
[7] R.J. Braun, Optimal Design and Operation of Solid Oxide Fuel Cell Systems for Small-scale Stationary Applications, PhD Thesis, University of Wisconsin-Madison, USA, 2002.
[8] Y. Matsuzake, I. Yasuda, J. Electrochem. Soc. 147 (2000) 1630.
[9] H. Yakabe, T. Ogiwara, M. Hishinuma, I. Yasuda, J. Power Sources 102 (2001) 144.
[10] Fluent User's Guide, Version 6.1, Fluent Inc., Lebanon, NH, 2003.
[11] J.R. Ferguson, J.M. Fiard, R. Herbin, J. Power Sources 58 (1996) 106.
[12] E. Achenbach, SOFC stack modeling, Final Report of Activity A2, Annex II: Modeling and Evaluation of Advanced Solid Oxide Fuel Cells, International Energy Agency Programme on R, D&D on Advanced Fuel Cells, Juelich, Germany, 1996.